Coplanar Waveguide and Slot Line on Magnetic Substrates: Analysis and Experiment

EL-BADAWY EL-SHARAWY AND ROBERT W. JACKSON, MEMBER, IEEE

Abstract—**A full-wave analysis is presented for coplanar waveguide and slot line phase shifters on magnetic substrates. The analysis is based on a Green's function which is formulated using a transmission matrix approach. Different configurations are investigated with respect to their nonreciprocal phase shift properties. Measurements are presented for a coplanar waveguide etched on the surface of a rectangular ferrite toroid. Calculated and measured results are in good agreement.**

I. Introduction

DUE TO THE recent progress in the growth and deposition of magnetic films on semiconductors [1], there is renewed interest in the characteristics of printed transmission lines on magnetized substrates. Printed structures are attractive due to their low fabrication costs and their compatibility with integrated circuits. In particular, coplanar waveguide is easy to construct and capable of very broad bandwidth connections with coaxial line. It is also somewhat similar to slot line in terms of field ellipticity and tendency to interact with magnetic material. In this paper, we present an analysis of differential phase shift in coplanar waveguide (CPW) and slot line on transversely magnetized substrates. These calculations are then verified experimentally for CPW printed on rectangular ferrite toroids.

Previous studies in this area have primarily been either theoretical or experimental for slot lines and CPW. Early work by Allen and Robinson [2] involved measurements of slot line on YIG substrates. At about the same time, Wen [3] measured differential phase shift for coplanar waveguide on YIG. Theoretical investigations have been widely reported [4]–[9] for slot line. CPW was analyzed by Kaneki [8] assuming very narrow slot width $W \ll \lambda$, but no curves were published. Several multilayer structures have been suggested [2], [7], [9], [10] with the intention of increasing the nonreciprocity of the slot line, but their effect on CPW is not clear.

The work presented here is primarily concerned with coplanar waveguide on magnetic substrates. A full-wave analysis is used to determine the effect of various configurations on differential phase shift. The analysis can be used for substrates of infinite width or for those confined by sidewalls. In this respect, it differs from our earlier work [11], which did not include sidewall effects. We subsequently found this to be important in accurately predicting the measurements which will be presented.

In what follows, the multilayer Green's function is formulated using a transmission matrix approach. This approach has been modified such that its computational efficiency is increased by deriving the transmission matrices for dielectric and ferrite slabs in a closed form. The Green's function is then applied to the full-wave analysis of a slot line and CPW on infinite width substrates. Several different multilayered configurations are investigated. Next, perfectly conducting sidewalls are added to the analysis. The resulting configuration is used to study the effect of various CPW parameters on differential phase shift. Finally, an experimental structure built on a ferrite toroid will be described and differential phase analysis compared to measurements.

II. Green's Function Formulation Using the Transmission Matrix

In this section, the multilayer structure shown in Fig. 1a is considered. A Green's function in the Fourier transform domain is derived which relates the transformed tangential electric fields $\tilde{\boldsymbol{E}}$ on one surface to the transformed electric surface currents $\tilde{\boldsymbol{J}}$, on the same surface. This relationship has the form

$$\tilde{\boldsymbol{J}}(k_x, k_y) = \tilde{\bar{\boldsymbol{G}}}(k_x, k_y)\tilde{\boldsymbol{E}}(k_x, k_y) \tag{1}$$

where $\tilde{\bar{\boldsymbol{G}}}(k_x, k_y)$ is the Green's function in the Fourier transform domain and where the Fourier transform is defined by

$$\boldsymbol{E}(x, y) = \frac{1}{(2\pi)^2}\int_{-\infty}^{\infty}\int_{-\infty}^{\infty}\tilde{\boldsymbol{E}}(k_x, k_y)e^{jk_x x}e^{jk_y y}\,dk_x\,dk_y. \tag{2}$$

To find $\tilde{\bar{\boldsymbol{G}}}$, a 2×2 matrix, a transmission matrix approach will be employed which is somewhat similar to the approach suggested in [12]–[14]. Fig. 1b shows a slab, possibly magnetic, of thickness d with transformed electric fields and currents $\tilde{\boldsymbol{E}}_1$, $\tilde{\boldsymbol{J}}_1$, $\tilde{\boldsymbol{E}}_2$, $\tilde{\boldsymbol{J}}_2$ assumed at the boundaries with other layers. The transmission matrix, $\tilde{\bar{\boldsymbol{T}}}(d)$, is a 4×4

Manuscript received October 23, 1987; revised January 16, 1988. This work was supported by the Raytheon Company, Special Microwave Device Operation, Northborough, MA.

The authors are with the Department of Electrical and Computer Engineering, University of Massachutsetts, Amherst, MA 01003.

IEEE Log Number 8820442.

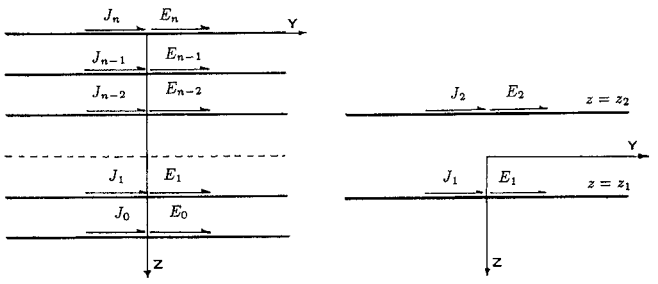

Fig. 1. Geometry of (a) single-layer and (b) multilayer structures.

matrix defined such that

$$\begin{bmatrix} \tilde{E}_2 \\ \tilde{J}_2 \end{bmatrix} = \left[\bar{\bar{T}}(d)\right] \begin{bmatrix} \tilde{E}_1 \\ \tilde{J}_1 \end{bmatrix} \tag{3}$$

where the tangential electric field components and the surface current components form a four-element vector. To find $\bar{\bar{T}}(d)$ we start from Maxwell's equations:

$$\nabla \times \boldsymbol{H} = j\omega\epsilon \boldsymbol{E} \qquad \nabla \times \boldsymbol{E} = -j\omega\bar{\mu}\cdot\boldsymbol{H}$$
$$\nabla\cdot(\bar{\mu}\cdot\boldsymbol{H}) = 0 \qquad \nabla\cdot\boldsymbol{E} = 0 \tag{4}$$

where $\bar{\mu}$ is the permeability tensor of the ferrite. For a ferrite magnetized in the y direction, the permeability tensor is [15]

$$\bar{\mu} = \begin{bmatrix} \mu & 0 & -j\kappa \\ 0 & \mu_0 & 0 \\ j\kappa & 0 & \mu \end{bmatrix} \tag{5}$$

and

$$\mu = \mu_0\left(1 + \frac{\bar{\omega}_0\omega_m}{\bar{\omega}_0^2 - \omega^2}\right) \qquad \kappa = \frac{\mu_0\omega\omega_m}{\bar{\omega}_0^2 - \omega^2},$$
$$\omega_m = \gamma 4\pi M_s \qquad \bar{\omega}_0 = \omega_0 + j/T \qquad \omega_0 = \gamma H_0$$

where ω_0 is the precession frequency, H_0 is the impressed dc magnetic field, γ is the gyromagnetic ratio, $T = 2/\gamma\Delta H$ is the relaxation time, and ΔH is the 3 dB line width. To simplify the formulation of the fields, the wave equations are expressed in terms of fields which are longitudinal to the direction of magnetization (y direction). The following equations determine $\tilde{E}_y$, $\tilde{H}_y$:

$$\frac{\partial^2\tilde{E}_y}{\partial z^2} - \left(k_x^2 + k_y^2 - \omega^2\epsilon\frac{\mu^2-\kappa^2}{\mu}\right)\tilde{E}_y = -j\omega\mu_0 k_y\frac{\kappa}{\mu}\tilde{H}_y$$
$$\frac{\partial^2\tilde{H}_y}{\partial z^2} - \left(k_x^2 + \frac{\mu_0}{\mu}k_y^2 - \omega^2\mu_0\epsilon\right)\tilde{H}_y = j\omega\epsilon k_y\frac{\kappa}{\mu}\tilde{E}_y \tag{6}$$

where $\tilde{E}_y$ and $\tilde{H}_y$ are functions of z and the Fourier variables k_x and k_y. The other field components can be expressed in terms of the y components, as

$$\tilde{E}^{\pm} = \frac{-jk_y\nabla^{\pm}E_y \pm \omega(\mu\pm\kappa)\nabla^{\pm}H_y}{k_y^2 - \omega^2\epsilon(\mu\pm\kappa)}$$
$$\tilde{H}^{\pm} = \frac{-jk_y\nabla^{\pm}H_y \mp \omega\epsilon\nabla^{\pm}E_y}{k_y^2 - \omega^2\epsilon(\mu\pm\kappa)} \tag{7}$$

where $\tilde{E}^{\pm}$, $\tilde{H}^{\pm}$ are elliptically polarized fields and can be written as

$$\tilde{E}^{\pm} = \tilde{E}_z \pm j\tilde{E}_x$$
$$\tilde{H}^{\pm} = \tilde{H}_z \pm j\tilde{H}_x \tag{8}$$

and

$$\nabla^{\pm} = \frac{\partial}{\partial z} \mp k_x. \tag{9}$$

If $k_y \neq 0$, (6) can be solved by assuming that $\tilde{E}_y$ and $\tilde{H}_y$ are proportional to each other as

$$\tilde{E}_y = j\eta\tilde{H}_y. \tag{10}$$

To justify assumption (10), $\tilde{E}_y$ and $\tilde{H}_y$ must have the same z dependence. The resulting equation in η is written as

$$k_y^2 - \omega^2\epsilon\frac{\mu^2-\kappa^2}{\mu} - \omega\mu_0 k_y\frac{\kappa}{\mu\eta} = \frac{\mu_0}{\mu}k_y^2 - \omega^2\mu_0\epsilon - \omega\epsilon k_y\frac{\kappa}{\mu}\eta \tag{11}$$

which has two roots of η_p and η_n. $\tilde{E}_y$ and $\tilde{H}_y$ can then be written in the form

$$\tilde{E}_y = j\eta_p\left[A_1\sinh(k_pz) + B_1\cosh(k_pz)\right] + j\eta_n\left[A_2\sinh(k_nz) + B_2\cosh(k_nz)\right]$$
$$\tilde{H}_y = A_1\sinh(k_pz) + B_1\cosh(k_pz) + A_2\sinh(k_nz) + B_2\cosh(k_nz) \tag{12}$$

where A_1, B_1, A_2, B_2 are arbitrary constants and

$$k_p = \left(k_x^2 + \frac{\mu_0}{\mu}k_y^2 - \omega^2\mu_0\epsilon - \eta_p\omega\epsilon k_y\frac{\kappa}{\mu}\right)^{1/2}$$
$$k_n = \left(k_x^2 + \frac{\mu_0}{\mu}k_y^2 - \omega^2\mu_0\epsilon - \eta_n\omega\epsilon k_y\frac{\kappa}{\mu}\right)^{1/2}. \tag{13}$$

This solution is similar to that given in [4]. Equations (12) and (13) show that there are two eigenwaves describing the fields in a homogeneous magnetized material.

At $z = z_1$, (7) and (12) can be used to write $\tilde{E}_1$, $\tilde{J}_1$ as

$$\begin{bmatrix} \tilde{E}_1 \\ \tilde{J}_1 \end{bmatrix} = \bar{\bar{M}}(z_1)\cdot\boldsymbol{A} \tag{14}$$

where

$$\boldsymbol{A} = \begin{bmatrix} A_1 \\ B_1 \\ A_2 \\ B_2 \end{bmatrix} \tag{15}$$

and $\bar{\bar{M}}$ is 4×4 matrix which relates $\tilde{E}_1$ and $\tilde{J}_1$ to the arbitrary constants. Similarly, $\tilde{E}_2$, $\tilde{J}_2$ can be expressed as

$$\begin{bmatrix} \tilde{E}_2 \\ \tilde{J}_2 \end{bmatrix} = \bar{\bar{M}}(z_2)\cdot\boldsymbol{A}. \tag{16}$$

From (12) and (14),

$$\begin{bmatrix} \tilde{E}_2 \\ \tilde{J}_2 \end{bmatrix} = \tilde{\bar{M}}(z_2)\cdot\tilde{\bar{M}}^{-1}(z_1)\cdot\begin{bmatrix} \tilde{E}_1 \\ J_1 \end{bmatrix} \tag{17}$$

and from (1) and (15),

$$\tilde{\bar{T}}(d) = \tilde{\bar{M}}(z_2)\cdot\tilde{\bar{M}}^{-1}(z_1). \tag{18}$$

The coordinates, z_1 and z_2, can be chosen arbitrarily such that $z_1 - z_2 = d$. However, to find the mathematical expression for $\tilde{\bar{T}}(d)$ and eliminate the necessity of inverting $\tilde{\bar{M}}$ numerically, z_1 is chosen to be zero and $z_2 = -d$. The elements of the matrix $\tilde{\bar{T}}$ for dielectric and ferrite slabs are listed in Appendix I and Appendix II, respectively.

Transmission matrices have the following useful properties:

$$\tilde{\bar{T}}(0) = \bar{I} \tag{19a}$$

$$\tilde{\bar{T}}(a+b) = \tilde{\bar{T}}(a)\tilde{\bar{T}}(b) \tag{19b}$$

$$\tilde{\bar{T}}(-d) = \tilde{\bar{T}}^{-1}(d) \tag{19c}$$

where $\bar{I}$ is the unity matrix. Property (19b) can be used to find the transmission matrix of a multilayer structure (see Fig. 1(a)) by multiplying the transmission matrices of the individual layers in the correct sequence.

To find the Green's function in (1), the total multilayer transmission matrix is partitioned as

$$\tilde{\bar{T}} = \begin{bmatrix} \tilde{\bar{T}}_E & \tilde{\bar{Z}}_T \\ \tilde{\bar{Y}}_T & \tilde{\bar{T}}_J \end{bmatrix} \tag{20}$$

where $\tilde{\bar{T}}_E, \tilde{\bar{Z}}_T, \tilde{\bar{Y}}_T, \tilde{\bar{T}}_J$ are 2×2 matrices. The first layer in Fig. 1(a) can then be made either a shielded layer or infinitely thick. When the first layer is shielded, the boundary condition $\tilde{E}_0 = 0$ can be used to determine the desired Green's function as

$$\tilde{\bar{G}} = \tilde{\bar{T}}_J\tilde{\bar{Z}}_T^{-1} \tag{21}$$

where $\tilde{\bar{G}}$ relates tangential $\tilde{J}$ to tangential $\tilde{E}$ on the nth layer (see Fig. 1(a)). For an infinite first layer, the Green's function is found by taking the limit of (21) as the thickness of the layer approaches infinity. A more efficient approach uses the semispace Green's function, $\tilde{\bar{G}}_1$, (see Appendix I) in place of the first layer. The total Green's function can then be written as

$$\tilde{\bar{G}} = \left(\tilde{\bar{Y}}_T + \tilde{\bar{T}}_J\tilde{\bar{G}}_1\right)\left(\tilde{\bar{T}}_E + \tilde{\bar{Z}}_T\tilde{\bar{G}}_1\right)^{-1} \tag{22}$$

where $\tilde{\bar{Y}}_T, \tilde{\bar{T}}_J, \tilde{\bar{T}}_E, \tilde{\bar{Z}}_T$ in this case are the submatrices of the transmission matrix for the multilayer structure excluding the first layer. This eliminates the necessity of taking the $d = \infty$ limit and somewhat reduces the number of transmission matrices to be found and the number of multiplications.

The solution for ferrite substrates is greatly simplified using the present approach due to the fact that it deals directly with the fields. This is in contrast to the published techniques [16]–[19] which use potential functions for the analysis of multilayer structures. Further simplification has been achieved through using (18) to find the transmission matrix instead of conventional techniques [12]–[14] in which an eigenvector matrix is constructed. As a result, the transmission matrices for single ferrite and dielectric slabs ($k_y \neq 0$) have been derived in a closed form.

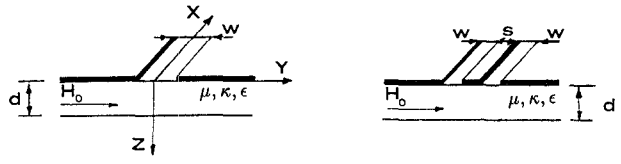

Fig. 2. Geometry of (a) slot line and (b) coplanar waveguide.

III. Slot Line and CPW on Infinitely Wide Substrate

A. Full-Wave Formulation

Fig. 2 shows the geometry of the slot line and CPW under consideration. The analysis of these structures is based upon the spectral-domain technique [20], [21]. A Green's function is used to find the electric surface current J in terms of the electric field $\tilde{E}$ as

$$J(y) = \frac{1}{2\pi}\int_{-\infty}^{\infty}\tilde{\bar{G}}(-\beta, k_y)\tilde{E}(k_y)e^{jk_y y}\,dk_y. \tag{23}$$

The boundary conditions ($J(y) = 0$ inside the slot) at the plane of the slot line or CPW are enforced by employing Galerkin's method.

In this work, the electric fields in a single slot are expanded according to [24]

$$E_y(y) = \sum_{n=0}^{N_y} c_n f_{yn}$$

$$E_x(y) = \sum_{n=0}^{N_x} d_n f_{xn} \tag{24}$$

where the expansion functions f_{yn} and f_{xn} are defined to be

$$f_{yn} = (-1)^n T_n\left(\frac{2y}{W}\right)\Big/\sqrt{1-\left(\frac{2y}{W}\right)^2} \tag{25a}$$

$$f_{xn} = (-1)^n U_n\left(\frac{2y}{W}\right)\sqrt{1-\left(\frac{2y}{W}\right)^2} \tag{25b}$$

and where W is the width of the slot and the functions T_n and U_n are Chebyshev polynomials of the first and second kinds, respectively. (These functions are similar to those used in [20], [21], but are more computationally efficient.) For a slot line, the longitudinal component is an odd function of y, whereas the transverse component is an even function of y. Therefore, only the even values of n are used in (25a) and only the odd values are used in (25b). For CPW, the entire set (odd and even) is used to account for the possible close coupling between the slots and that

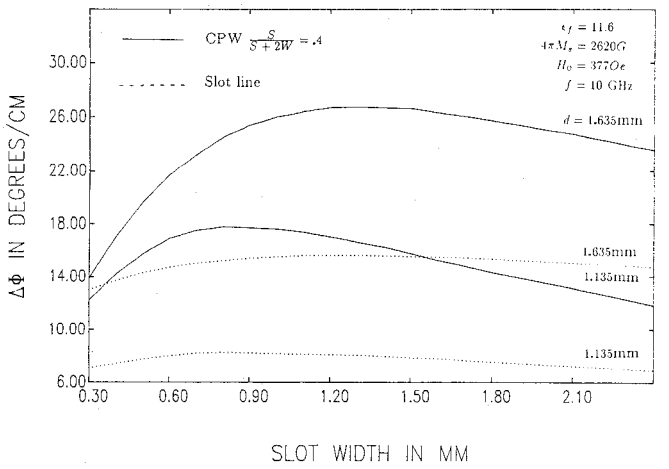

Fig. 3. Differential phase shift for slot line and coplanar waveguide on a single-layer of ferrite.

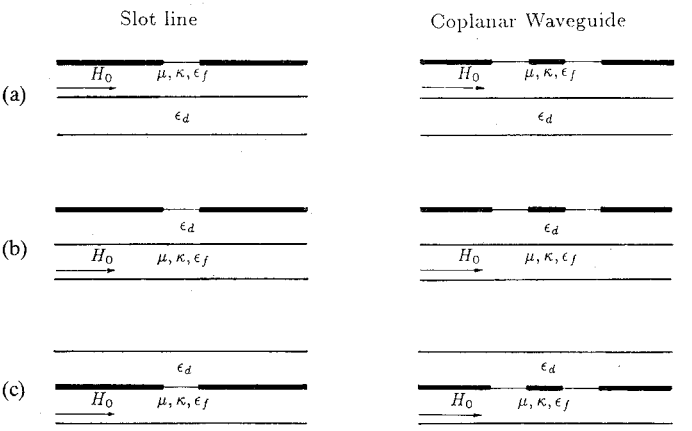

Fig. 4. Different configurations of a multilayer phase shifter. (a) Ferrite–dielectric substrate. (b) Dielectric–ferrite substrate. (c) Sandwich structure.

set is displaced to $y = \pm(S+W)/2$ with the symmetries which are proper for CPW.

Following the Galerkin procedure, $\boldsymbol{J}$ in (23) is tested with f_{xn} and f_{yn}, which results in an admittance matrix, $\overline{\boldsymbol{Y}}$, such that

$$\overline{\boldsymbol{Y}} = \begin{bmatrix} \overline{\boldsymbol{Y}}^{xx} & \overline{\boldsymbol{Y}}^{xy} \\ \overline{\boldsymbol{Y}}^{yx} & \overline{\boldsymbol{Y}}^{yy} \end{bmatrix} \tag{26}$$

and

$$Y_{m,n}^{pq} = \int_{-\infty}^{\infty} F_{pm}^{*}(k_y)\tilde{G}_{pq}(-\beta, k_y)F_{qn}(k_y)\,dk_y \tag{27}$$

where F_{pn} is the Fourier transform of the basis functions (25) written as

$$F_{yn} = j^n \frac{\pi W}{2} J_n\left(\frac{k_y W}{2}\right)$$

$$F_{xn} = j^n \frac{\pi W}{2}(n+1) J_{n+1}\left(\frac{k_y W}{2}\right) \Big/ \frac{k_y W}{2}. \tag{28}$$

For a particular value of β, the integrals in (27) are evaluated numerically. The values which force the determinant of $\overline{\boldsymbol{Y}}$ to zero are mode propagation constants. Nonreciprocal phase shift is defined to be the difference between the propagation constants of the forward $(+x)$ traveling and reverse $(-x)$ traveling modes, $\Delta\phi = \beta_f - \beta_r$ (°/cm). N_x and N_y in (24) are increased until $\Delta\phi$ is converged. Two or three functions for each field component are sufficient.

In evaluating $\overline{\boldsymbol{Y}}$, poles can occur in the numerical integration. These poles correspond to the various surface waves which can be supported in the structure. The integration takes place up to a pole and then continues on the other side (principal value). Residues should also be added to represent the leakage of energy from the fundamental mode into the parasitic waves of the structure. Since these waves are electromagnetic surface waves or magnetostatic surface waves, it is possible to avoid their excitation by a proper choice of substrate thickness and ferrite magnetization. For the applications presented here, the operating frequency range is such that magnetostatic surface waves [10], [22], [23] are cut off.

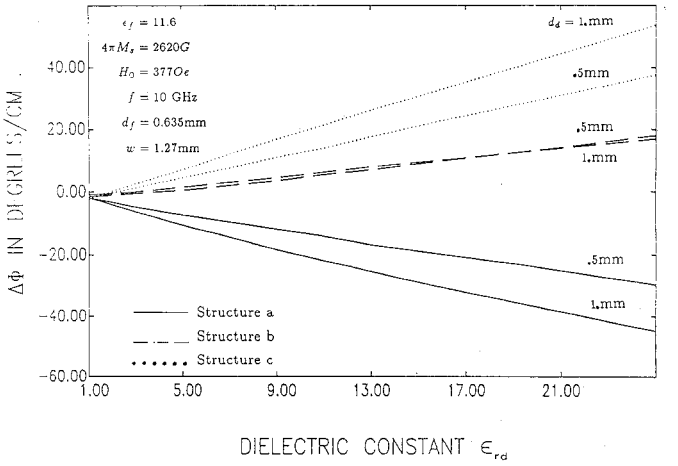

Fig. 5. Differential phase shift of a slot line in a multilayer structure.

B. Results

The differential phase shift for slot line and CPW is plotted in Fig. 3 versus the width of the slot for two different substrate thicknesses. For substrate thicknesses up to $0.1\lambda_0$ (larger thicknesses were not checked), differential phase shift was generally found to increase with substrate thickness in both slot line and CPW. Also, there is an optimum slot width for CPW which increases with increasing substrate thickness. In all results, we considered only the odd mode of the CPW because of its compatibility with coaxial feed. The figure also shows that the available differential phase shift from a CPW on a single layer of ferrite can be higher than that for a slot line.

Different configurations employing an additional layer of dielectric have been suggested [2], [7], [9] to improve the nonreciprocity of a slot line. Fig. 4 shows the three major structures, and Fig. 5 shows the nonreciprocal slot phase shift obtained from the three different structures versus the relative permittivity, ϵ_{rd}, of the dielectric layer for two different thicknesses of dielectric. For low and medium

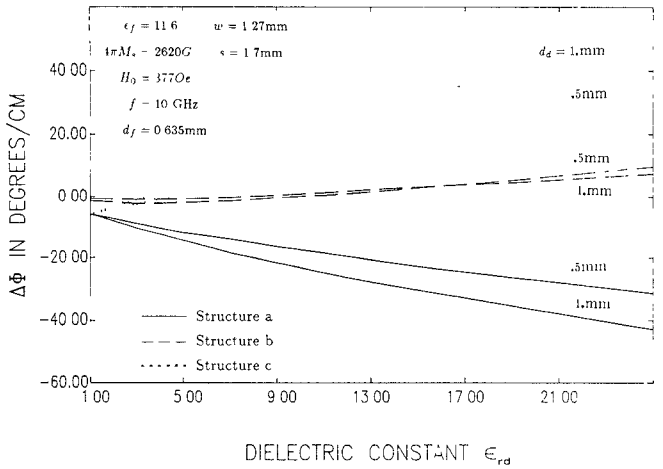

Fig. 6. Differential phase shift of a coplanar waveguide in a multilayer structure.

values of ϵ_{rd}, the best nonreciprocity is obtained from structure *a* whereas for high ϵ_{rd} the best nonreciprocity is obtained from structure *c*. Although the figure does not show it, structures *a* and *b* have an optimum dielectric thickness for some values of ϵ_{rd}. This is in agreement with the conclusions reached in [7] and [9]. Note also that the phase shift presented in Fig. 5 for $\epsilon_{rd} = 20$ is in agreement with results presented in [7]. All three structures have been examined for other ferrite substrates. In structures *b* and *c*, the differential phase shift can equal zero at specific values of ϵ_{rd}. This value decreases with increasing magnetization and applied dc magnetic field. On the other hand, structure *a* seems to offer high nonreciprocity over a wide variety of ferrite and dielectric substrates.

Figs. 3 and 5 show the usefulness of structure *a*. Two layers of ferrite and dielectric having the same permittivity can offer higher nonreciprocity than a single layer of ferrite with thickness equal to the combined thicknesses of the two layers. This can be explained by the fact that the field ellipticities at the upper and lower boundaries with air counteract each other for a single layer of ferrite. When air at one of these boundaries is replaced by a dielectric, especially of high permittivity, the counteracting elliptical field is moved out of the ferrite toward the new air–dielectric interface.

The effect of an extra layer on a CPW is similar to what was observed for a slot line. Fig. 6 shows the differential phase shift for the same three configurations as in Fig. 5. Structure *a* produces higher differential phase shift for low and medium ϵ_{rd} than the same set of layers in a slot line, whereas structure *b* shows less phase shift than the corresponding slot line.

IV. Slot Line and CPW on Ferrite Substrates with Conducting Walls

A. Full-Wave Formulation

The geometry of slot line and CPW with perfectly conducting sidewalls is shown in Fig. 7. The $\hat{y}$-directed

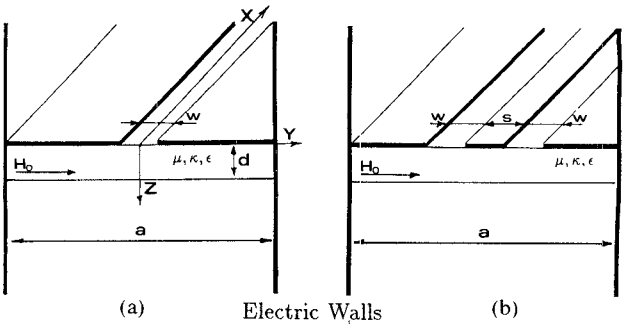

Fig. 7. Geometry of (a) a slot line and (b) a coplanar waveguide with conducting sidewalls.

electric and magnetic fields can be written in the form

$$E_y(x,y) = \frac{1}{2\pi}\int_{-\infty}^{\infty} e^{jk_x x} \sum_{n=-\infty}^{\infty} \tilde{E}_y(k_x, k_{yn}) e^{jk_{yn}y}\, dk_x \tag{29a}$$

$$H_y(x,y) = \frac{1}{2\pi}\int_{-\infty}^{\infty} e^{jk_x x} \sum_{n=-\infty}^{\infty} \tilde{H}_y(k_x, k_{yn}) e^{jk_{yn}y}\, dk_x \tag{29b}$$

where k_{yn} is discrete. Applying (29) to the procedure described by (3)–(22) results in the expression

$$\boldsymbol{J}(y) = \sum_{n=-\infty}^{\infty} \tilde{\bar{\boldsymbol{G}}}(-\beta, k_{yn})\tilde{\boldsymbol{E}}(k_{yn}) e^{jk_{yn}y} \tag{30}$$

where $\tilde{\bar{\boldsymbol{G}}}$ is exactly the same function as in (23) and $\tilde{\boldsymbol{E}}$ and $\boldsymbol{J}$ correspond to the tangential electric field and current on the $z = 0$ surface.

In order for the electric field boundary conditions to be satisfied at $y = \pm a/2$, the values of k_{yn} are constrained to be $n\pi/a$ and

$$\tilde{E}_y(k_{yn}) = (-1)^n \tilde{E}_y(-k_{yn}) \tag{31a}$$

$$\tilde{E}_x(k_{yn}) = -(-1)^n \tilde{E}_x(-k_{yn}). \tag{31b}$$

For a slot line, E_y must be an even function of y and E_x must be odd. This and equations (31) imply that n in (29) and (30) takes on only even values. For a CPW, E_y is an odd function of y and E_x is even, which results in n taking only odd values.

The fields in (30) are then expanded in terms of the functions described previously. As before, these same functions are used to test that the currents in the slots are zero. The elements of the resulting admittance matrix are given by

$$Y_{ij}^{pq} = \sum_n F_{pi}^*\left(\frac{n\pi}{a}\right)\tilde{G}_{pq}\left(-\beta, \frac{n\pi}{a}\right)F_{qj}\left(\frac{n\pi}{a}\right) \tag{32}$$

where n is even for slot line analysis and odd for CPW. The propagation constant(s) is the value of β which makes $|\bar{Y}| = 0$.

The poles of $\tilde{\bar{\boldsymbol{G}}}$, corresponding to surface waves in the no-sidewall case, generate other solutions for β. In the case of a slot line with sidewalls, these modes correspond to the finline modes known as FD and FM modes in [4].

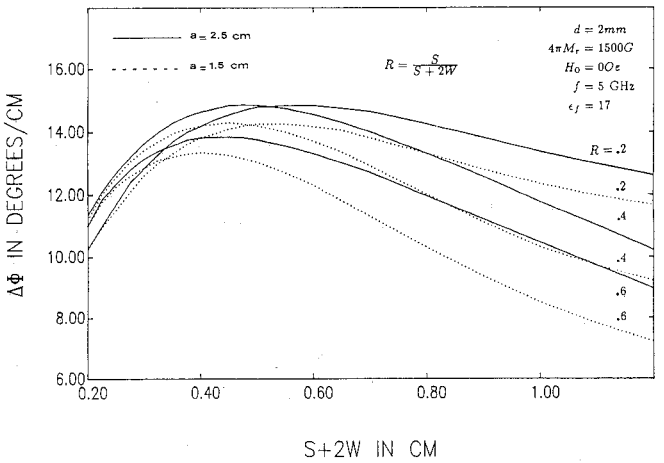

Fig. 8. Differential phase shift of a coplanar waveguide with electric walls.

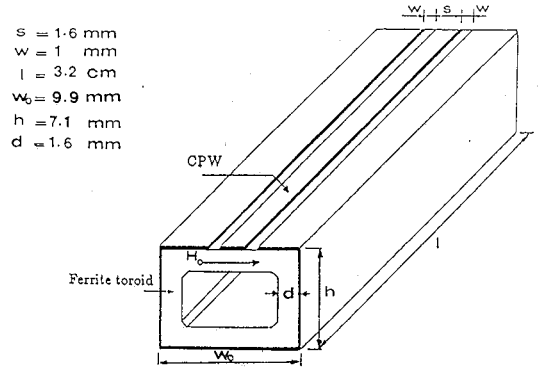

Fig. 9. Ferrite toroid with CPW on the surface.

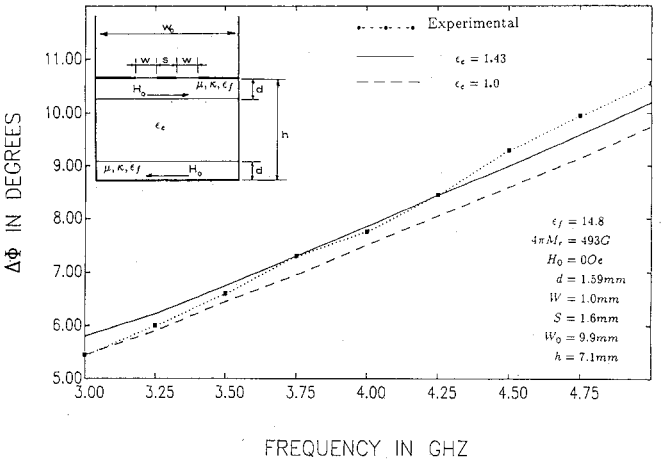

Fig. 10. Measured and calculated differential phase shift of a CPW on the surface of a toroid.

B. Results

The dispersion characteristics of a slot line confined by electric walls have been calculated using the formulation described above. Good agreement (at worst, a 5 percent difference in propagation constant) with other published results [4] was obtained. Sidewall proximity has a noticeable effect on slot line nonreciprocity, reducing it significantly. For example, if the slot analyzed in Fig. 3 is enclosed by sidewalls separated by 1.5 cm, the peak phase shift is reduced by 50 percent.

Sidewall proximity also has an effect on the nonreciprocity of CPW but much less than for a slot line. If sidewalls, again separated by 1.5 cm, confine the CPW analyzed in Fig. 3, the phase shift is reduced by only 6 percent. This reduced sensitivity can be explained by the odd symmetry of the CPW fields. The resulting field decay with increased y is more pronounced than the single slot field decay. Therefore, changing the sidewall location perturbs the CPW fields less than it perturbs the slot field.

Fig. 8 shows the calculated differential phase of a latched CPW versus total CPW size $(S+2W)$ for various aspect ratios and sidewall proximities. Note that, for a particular aspect ratio, there is an optimum CPW size. This also occurred in the CPW without sidewalls. Differential phase shift can be further increased by increasing the substrate thickness or by using multilayer configurations, as mentioned in Section III.

V. Experimental Verification

In this section, measurements are presented for the differential phase shift between the two latched states of a coplanar waveguide etched on the metallized wall of a rectangular ferrite toroid (see Fig. 9). Toroidal structures such as these are used extensively in waveguide phase shifters and are particularly attractive because the closed magnetic path allows for easy biasing. The ferrite material used in these measurements was TRANSTECH G-1004 having a nominal remanent magnetization of 493 gauss. The outer dimensions of the toroid are $9.9\times7.1\times31.8$ mm with a wall thickness of 1.59 mm. The entire outside surface of the toroid was gold-plated. A coplanar waveguide, etched in the broad wall, had outside dimensions of 3.6 mm and an aspect ratio of 0.444. The structure was modeled as two horizontal ferrite slabs between two vertical electric walls separated by the broad wall width (see figure inset). In this model, the effect of the ferrite vertical walls was neglected initially, so that the two horizontal slabs are separated by an air gap. Fig. 10 shows the measured versus calculated differential phase shift. Reasonably good agreement is observed, with the worst discrepancy, about 0.8°, occurring at 5 GHz.

The effect of the ferrite sidewalls may be approximately taken into account by replacing the air gap in the previous model with a dielectric layer as shown in Fig. 10. The effective dielectric constant ϵ_e of this layer was calculated from the following relation:

$$\epsilon_e = \left(1 - \frac{2d(\epsilon_f - 1)}{W_o \epsilon_f}\right)^{-1} \tag{33}$$

where ϵ_f is the ferrite dielectric constant, d is the toroid wall thickness, and W_o is the toroid outer width. A plot for the calculated phase difference using this approximation

($\epsilon_e = 1.43$) is shown in Fig. 10. An improvement in the accuracy of the model results.

A second CPW was built on an identical toroid. This CPW was larger ($S = 2.4$ mm, $W = 1.7$ mm) than the first one and gave almost the same differential phase shift over a frequency range between 3 and 5 GHz. Measured and calculated results agreed within 14 percent. This higher discrepancy is probably due to the close proximity of the CPW to the ferrite vertical walls.

The aspect ratios in both cases were chosen to give roughly a 50 Ω impedance. Return loss in the first case was roughly 15 dB with a 1–2 dB insertion loss. The second case gave a worse match due to poor contacts at the input and output of the CPW.

We note that our previous analytical work on this configuration [11] gave worse agreement with measurements. This was due to the assumption that the conducting sidewalls had no effect on phase shift. Our present work shows that the sidewall can introduce significant effects.

VI. Conclusions

A full-wave analysis of coplanar waveguide and slot line on magnetic substrates has been formulated using a transmission matrix technique. The analysis was then used to study a number of configurations in order to determine the factors which influence the nonreciprocity. Using a dielectric layer in addition to the ferrite layer was shown to be a useful method for increasing phase shift. Optimum dimensions for maximum nonreciprocity in coplanar waveguide and slot line were found to exist. A reduction in phase shift was found to occur due to the presence of conducting sidewalls, and this effect was more pronounced in slot line than in coplanar waveguide. Coplanar waveguide gave as good or better nonreciprocity than slot line in the configurations which were studied.

In order to verify the analysis, phase shift measurements were made for a coplanar waveguide printed on the broad wall of a rectangular toroid. Good agreement between calculated and measured phase shift was observed.

The results presented in this paper, along with the prospect of coaxial compatibility, show coplanar waveguide to be a promising nonreciprocal medium.

Appendix I

The submatrices of the transmission matrix for dielectric slab are expressed as

$$\bar{\bar{T}}_E = \bar{\bar{T}}_J = \cosh kd \begin{bmatrix} 1 & 0 \\ 0 & 1 \end{bmatrix} \tag{A1}$$

$$\bar{\bar{Z}}_T = \frac{jZ_c}{kk_d} \sinh kd \begin{bmatrix} k_x^2 - k_d^2 & k_x k_y \\ k_x k_y & k_y^2 - k_d^2 \end{bmatrix} \tag{A2}$$

$$\bar{\bar{Y}}_T = \frac{jY_c}{kk_d} \sinh kd \begin{bmatrix} k_y^2 - k_d^2 & -k_x k_y \\ -k_x k_y & k_x^2 - k_d^2 \end{bmatrix} \tag{A3}$$

where

$$k = \left(k_x^2 + k_y^2 - k_d^2\right)^{1/2}$$
$$k_d = \omega\sqrt{\mu_0 \epsilon}$$
$$Z_c = \frac{1}{Y_c} = \sqrt{\frac{\mu_0}{\epsilon}}. \tag{A4}$$

From (A2) and (A3) we note that $|\bar{\bar{Z}}_T| = (Z_c \sinh kd)^2$, $|\bar{\bar{Y}}_T| = (Y_c \sinh kd)^2$, and

$$\frac{\bar{\bar{Z}}_T}{\sinh kd} = \left(\frac{\bar{\bar{Y}}_T}{\sinh kd}\right)^{-1}. \tag{A5}$$

The semispace Green's function, $\bar{\bar{G}}$, in (22), is

$$\bar{\bar{G}} = \frac{jY_c}{kk_d} \begin{bmatrix} k_y^2 - k_d^2 & -k_x k_y \\ -k_x k_y & k_x^2 - k_d^2 \end{bmatrix}. \tag{A6}$$

Appendix II

The submatrices of the transmission matrix for a magnetic slab with H_0 in the y direction are

$$\bar{\bar{T}}_E(1,1) = C_1 D_3 + C_5 D_4$$

$$\bar{\bar{T}}_E(1,2) = -j\frac{D_1 - D_2}{\eta_p - \eta_n} + C_2 D_3 + C_6 D_4$$

$$\bar{\bar{T}}_E(2,1) = -j\left(\eta_p C_1 \sinh k_p d + \eta_n C_5 \sinh k_n d\right)$$

$$\bar{\bar{T}}_E(2,2) = \frac{\eta_p \cosh k_p d - \eta_n \cosh k_n d}{\eta_p - \eta_n} - j\left(\eta_p C_2 \sinh k_p d + \eta_n C_6 \sinh k_n d\right)$$

$$\bar{\bar{Z}}_T(1,1) = \frac{\eta_n D_1 - \eta_p D_2}{\eta_p - \eta_n} + C_3 D_3 + C_7 D_4$$

$$\bar{\bar{Z}}_T(1,2) = C_4 D_3 + C_8 D_4$$

$$\bar{\bar{Z}}_T(2,1) = j\frac{\eta_p \eta_n}{\eta_p - \eta_n}\left(\cosh k_p d - \cosh k_n d\right) - j\left(\eta_p C_3 \sinh k_p d + \eta_n C_7 \sinh k_n d\right)$$

$$\bar{\bar{Z}}_T(2,2) = -j\left(\eta_p C_4 \sinh k_p d + \eta_n C_8 \sinh k_n d\right)$$

$$\bar{\bar{Y}}_T(1,1) = C_1 \sinh k_p d + C_5 \sinh k_n d$$

$$\bar{\bar{Y}}_T(1,2) = j\frac{\cosh k_p d - \cosh k_n d}{\eta_p - \eta_n} + C_2 \sinh k_p d + C_6 \sinh k_n d$$

$$\bar{\bar{Y}}_T(2,1) = C_1 D_7 + C_5 D_8$$

$$\bar{\bar{Y}}_T(2,2) = -j\frac{D_5 - D_6}{\eta_p - \eta_n} + C_2 D_7 + C_6 D_8$$

$$\tilde{\tilde{T}}_J(1,1) = -\frac{\eta_n \cosh k_p d - \eta_p \cosh k_n d}{\eta_p - \eta_n} + C_3 \sinh k_p d + C_7 \sinh k_n d$$

$$\tilde{\tilde{T}}_J(1,2) = C_4 \sinh k_p d + C_8 \sinh k_n d$$

$$\tilde{\tilde{T}}_J(2,1) = \frac{\eta_n D_5 - \eta_p D_6}{\eta_p - \eta_n} + C_3 D_7 + C_7 D_8$$

$$\tilde{\tilde{T}}_J(2,2) = C_4 D_7 + C_8 D_8 \tag{A7}$$

where

$$C_1 = \frac{j}{D}\beta_f^4 k_n \left(k_y \omega^2 \epsilon\kappa + \omega\epsilon\beta_h^2 \eta_n\right)$$

$$C_2 = -\frac{jk_n}{D}\left(k_x k_y \beta_h^2 \left(k_y \omega^2 \epsilon\kappa + \omega\epsilon\beta_h^2 \eta_n\right) - \omega\epsilon k_x \omega^2 \epsilon\kappa \left(k_y \omega^2 \epsilon\kappa \eta_n + \omega\mu\beta_e^2\right)\right)$$

$$C_3 = -\frac{k_x k_y k_n}{D}\left(\omega\kappa k_y \left(k_y \omega^2 \epsilon\kappa + \omega\epsilon\beta_h^2 \eta_n\right) - \beta_h^2 \left(k_y \omega^2 \epsilon\kappa \eta_n + \omega\mu\beta_e^2\right)\right)$$

$$C_4 = \frac{\beta_f^4}{D} k_n \left(k_y \omega^2 \epsilon\kappa \eta_n + \omega\mu\beta_e^2\right)$$

$$C_{i+4} = -C_i(n \to p), \qquad i = 1,2,3,4$$

$$D = k_p k_n (\eta_p - \eta_n)\omega^2 \mu\epsilon \left(k_y^2 \omega\epsilon\kappa \frac{\kappa}{\mu} - \beta_e^2 \beta_h^2\right)$$

$$D_1 = \frac{j}{\beta_f^4}\left(k_x k_y \left(\beta_h^2 \eta_p + \omega\kappa k_y\right)\cosh k_p d + k_p \left(\omega\mu\beta_e^2 + \omega^2 \epsilon\kappa k_y \eta_p\right)\sinh k_p d\right)$$

$$D_3 = -\frac{j}{\beta_f^4}\left(k_x k_y \left(\beta_h^2 \eta_p + \omega\kappa k_y\right)\sinh k_p d + k_p \left(\omega\mu\beta_e^2 + \omega^2 \epsilon\kappa k_y \eta_p\right)\cosh k_p d\right)$$

$$D_5 = \frac{1}{\beta_f^4}\left(k_p \left(\beta_h^2 \omega\epsilon\eta_p + \omega^2 \epsilon\kappa k_y\right)\sinh k_p d + k_x \left(k_y \beta_h^2 + \omega^2 \epsilon\kappa\omega\epsilon\eta_p\right)\cosh k_p d\right)$$

$$D_7 = -\frac{1}{\beta_f^4}\left(k_p \left(\beta_h^2 \omega\epsilon\eta_p + \omega^2 \epsilon\kappa k_y\right)\cosh k_p d + k_x \left(k_y \beta_h^2 + \omega^2 \epsilon\kappa\omega\epsilon\eta_p\right)\sinh k_p d\right)$$

$$D_{i+1} = D_i(p \to n), \qquad i = 1,3,5,7$$

$$\beta_f^4 = \left(k_y^2 - \omega^2\mu\epsilon\right)^2 - \left(\omega^2 \epsilon\kappa\right)^2$$

$$\beta_h^2 = k_y^2 - \omega^2\mu\epsilon$$

$$\beta_e^2 = k_y^2 - \omega^2 \epsilon \frac{\mu^2 - \kappa^2}{\mu}. \tag{A8}$$

REFERENCES

[1] "Workshop on Magnetic Materials," IEEE MTT Symp., 1986.

[2] G. Robinson and J. Allen, "Slot line application to miniature ferrite devices," *IEEE Trans. Microwave Theory Tech.*, vol. MTT-17, pp. 1037–1101, Dec. 1969.

[3] C. P. Wen, "Coplanar waveguide: A surface strip transmission line suitable for non-reciprocal gyromagnetic device applications," *IEEE Trans. Microwave Theory Tech.*, vol. MTT-7, pp. 1087–1090, Dec. 1969.

[4] F. Lange, "Analysis of shielded strip and slot lines on a ferrite substrate transversely magnetized in the plane of the substrate," *Arch. Elek. Übertragung.*, Band 36, Heft 3, pp. 95–100, Mar. 1982.

[5] Y. Hayashi and R. Mittra, "An analytical investigation of finlines with magnetized ferrite substrate," *IEEE Trans. Microwave Theory Tech.*, vol. MTT-31, pp. 495–498, June 1983.

[6] G. Böck, "Dispersion characteristics of slot line on ferrite substrate by a mode matching technique," *Electron. Lett.*, vol. 18, no. 12, pp. 536–537, Mar. 1982.

[7] G. Böck, "New multilayered slot line structures with high non-reciprocity," *Electron. Lett.*, vol. 19, no. 23, pp. 966–968, Nov. 1983.

[8] T. Kaneki, "Phase constants of the slot line and coplanar waveguide with ferrite substrates," *Denshi Trushin Gakki Ronbunski*, vol. 55, pp. 21–22, 1972.

[9] M. Geshiro and T. Itoh, "Analysis of double layered finlines containing a magnetized ferrite," in *Proc. IEEE MTT Symp.*, 1987, pp. 743–744.

[10] G. Harrison, G. Robinson, B. Savage, and D. Taft, "Ferrimagnetic parts for microwave integrated circuits," *IEEE Trans. Microwave Theory Tech.*, vol. MTT-19, pp. 577–587, July 1971.

[11] E. El-Sharawy and R. W. Jackson, "Full wave analysis of slot line and coplanar waveguide on a magnetic substrate," in *Proc. IEEE MTT Symp.*, 1987, pp. 993–995.

[12] C. Krowne, "Fourier transformed matrix method of finding propagation characteristics of complex anisotropic layered media," *IEEE Trans. Microwave Theory Tech.*, vol. MTT-32, pp. 1617–1625, Nov. 1984.

[13] D. Berreman, "Optics in stratified and anisotropic media: 4×4-matrix formulation," *J. Opt. Soc. Amer.*, vol. 62, no. 4, pp. 502–510, Apr. 1972.

[14] S. Teitler and B. Henvis, "Refraction in stratified, anisotropic media," *J. Opt. Soc. Amer.*, vol. 60, no. 6, pp. 830–834, June 1970.

[15] B. Lax and K. Button, *Microwave Ferrites and Ferromagnetics*. New York: McGraw-Hill, 1962.

[16] J. Davies and D. Syahkal, "Spectral domain solution of arbitrary coplanar transmission line with multilayer substrate," *IEEE Trans. Microwave Theory Tech.*, vol. MTT-25, pp. 143–146, Feb. 1977.

[17] R. Vahldieck and J. Bornemann, "A modified mode-matching technique and its application to a class of quasi-planar transmission lines," *IEEE Trans. Microwave Theory Tech.*, vol. MTT-33, pp. 916–925, Oct. 1985.

[18] R. Vahldieck, "Accurate hybrid mode analysis of various finline configurations including multilayered dielectrics, finite metallization thickness, and substrate holding grooves," *IEEE Trans. Microwave Theory Tech.*, vol. MTT-32, pp. 1454–1460, Nov. 1984.

[19] N. Das and D. Pozar, "A generalized spectral-domain Green's function for multilayer dielectric substrates with application to multilayer transmission lines," *IEEE Trans. Microwave Theory Tech.*, vol. MTT-35, pp. 326–335, Mar 1987.

[20] R. H. Jansen, "Unified user oriented computation of shielded, covered and open planar microwave and millimeter-wave transmission line characteristics," *Microwave, Opts. Acoust.*, vol. 3, no. 1, pp. 14–22, Jan. 1979.

[21] R. W. Jackson, "Consideration in the use of coplanar waveguide for millimeter-wave integrated circuits," *IEEE Trans. Microwave Theory Tech.*, vol. MTT-34, pp. 1450–1456, Dec. 1986.

[22] S. R. Seshadri, "Surface magnetostatic modes of a ferrite slab," *Proc. IEEE*, pp. 506–507, Mar. 1970.

[23] J. D. Adam, "A slot line MSW signal to noise enhancer," *IEEE Trans. Magn.* vol. 21, no. 5, pp. 1794–1796, Sept. 1985.

[24] R. Janaswamy and D. H. Schaubert, "Dispersion characteristics for wide slot lines on low permittivity substrates," *IEEE Trans. Microwave Theory Tech.*, vol. MTT-33, pp. 723–726, Aug. 1985.

El-Badawy El-Sharawy was born on October 18, 1957, in Mansoura, Egypt. He received the B.Sc. and M.Sc. degrees (with honors) in electrical engineering from Mansoura University, Egypt, in 1980 and 1984, respectively. He is currently a Ph.D. student at the University of Massachusetts. His current research interest is in the area of ferrite phase shifters.

Mr. El-Sharawy is a member of Eta Kappa Nu.

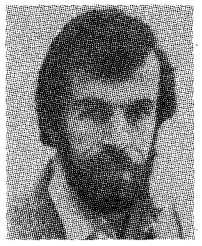

Robert W. Jackson (M'82) was born in Boston, MA, on October 18, 1952. He received the B.S. (1975) and Ph.D. (1981) degrees in electrical engineering from Northeastern University, Boston, MA. His thesis was on nonlinear plasma interactions in the earth's bow shock.

From 1981 to 1982 he was an Assistant Professor at Northeastern University. Since 1982 he has been on the faculty of the Department of Electrical and Computer Engineering at the University of Massachusetts, Amherst, where he is a member of the Microwave and Electronics Laboratory. His research interests include numerical electromagnetics applied to millimeter-wave integrated circuits and active microwave and millimeter-wave circuit design.